JOURNAL OF GEOPHYSICAL RESEARCH, VOL. 106, NO. B8, PAGES 16,145–16,161, AUGUST 10, 2001

Submersible study of an oceanic megamullion in the central North Atlantic

Brian E. Tucholke,[1] Kantaro Fujioka,[2] Takemi Ishihara,[3,4] Greg Hirth,[1] and Masataka Kinoshita[5,6]

Abstract. Recently discovered megamullions on the seafloor have been interpreted to be the exhumed footwalls of long-lived detachment faults operating near the ends of spreading segments in slow spreading crust. We conducted five submersible dives on one of these features just east of the rift valley in the Mid-Atlantic Ridge at 26°35′N and obtained visual, rock sample, gravity, and heat flow data along a transect from the breakaway zone (where the fault is interpreted to have first nucleated in ~2.0–2.2 Ma crust) westward to near the termination (~0.7 Ma). Our observations are consistent with the detachment fault hypothesis and show the following features. In the breakaway zone, faulted and steeply backtilted basaltic blocks suggest rotation above a deeper shear zone; the youngest normal faults in this sequence are interpreted to have evolved into the long-lived detachment fault. In younger crust the interpreted detachment surface rises as monotonously flat seafloor in a pair of broad, gently sloping domes that formed simultaneously along isochrons and are now thinly covered by sediment. The detachment surface is locally littered with basaltic debris that may have been clipped from the hanging wall. The domes coincide with a gravity high that continues along isochrons within the spreading segment. Modeling of on-bottom gravity measurements and recovery of serpentinites imply that mantle rises steeply and is exposed within ~7 km west of the breakaway but that rocks with intermediate densities prevail farther west. Within ~5 km of the termination, small volcanic cones appear on the detachment surface, indicating melt input into the footwall. We interpret the megamullion to have developed during a phase of limited magmatism in the spreading segment, with mantle being exhumed by the detachment fault <0.5 m.y. after its initiation. Increasing magmatism may eventually have weakened the lithosphere and facilitated propagation of a rift that terminated slip on the detachment fault progressively between ~1.3 m.y. and 0.7 m.y. Identifiable but low-amplitude magnetic anomalies over the megamullion indicate that it incorporates a magmatic component. We infer that much of the footwall is composed of variably serpentinized peridotite intruded by plutons and dikes.

1. Introduction

Mid-ocean ridges that have limited magma supply are strongly affected by normal faulting that creates rough abyssal hill topography. The largest fault scarps occur toward the ends of spreading segments [*Shaw*, 1992] but are concentrated at "inside corner" (IC) locations bounded on two edges by active plate boundaries: the spreading axis and the adjacent transform or nontransform offset [*Tucholke and Lin*, 1994]. IC fault scarps average several hundred meters high, and fault scarps are somewhat smaller on outside corner crust (OC) (conjugate to IC locations) and at segment centers [*Jaroslow*, 1997]. Recent studies, however, have identified what appear to be very large offset (~10–20 km) normal faults in IC settings within the Atlantic and Indian Oceans [*Tucholke et al*., 1996, 1998; *Cann et al*., 1997; *Mitchell et al*., 1998]. Long-lived slip on these major "detachment" faults is thought to be responsible for formation of distinctive footwall edifices termed megamullions.

Megamullions have two prominent characteristics: (1) a gently domed, overall turtleback shape (i.e., megamullion) and (2) a surface that is interpreted to be a single and extensive fault plane that is distinguished by the presence of prominent corrugations (mullion structures) that parallel the fault slip direction (e.g., Figures 1 and 2). In the direction of fault slip the updip limit of a megamullion is a breakaway zone where the fault initially nucleated. The downdip limit, or termination, normally is marked by contact with a hanging wall. Most known megamullions are fossil features on mid-ocean ridge flanks, where the hanging wall appears to be a remnant of rift floor crust that was stranded on the megamullion side of the rift by a small ridge jump or by formation of a younger, inboard fault within the rift valley. A few megamullions appear currently to be forming by slip on active boundary faults at the

[1]Department of Geology and Geophysics, Woods Hole Oceanographic Institution, Woods Hole, Massachusetts.
[2]Japan Marine Science and Technology Center, Yokusuka, Japan.
[3]Geological Survey of Japan, Tsukuba, Japan.
[4]Now at Institute for Marine Resources and Environment, National Institute for Advanced Industrial Science and Technology, Tsukuba, Japan.
[5]School of Marine Science and Technology, Tokai University, Shimizu-City, Japan.
[6]Now at Japan Marine Science and Technology Center, Yokusuka, Japan.

Paper number 2001JB000373.
0148-0227/01/2001JB000373$09.00

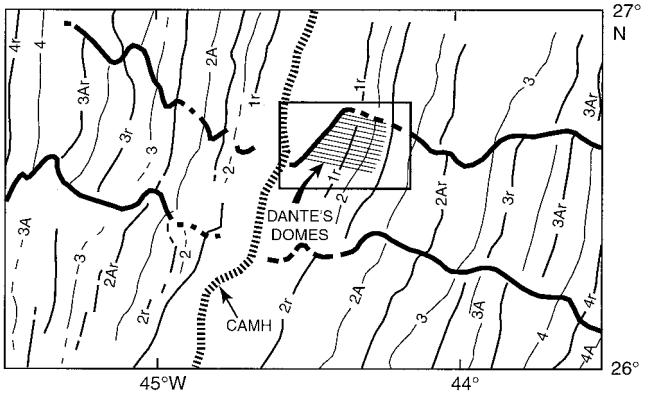

Figure 1. Location map of Dante's Domes megamullion (hatched) on the east flank of the Mid-Atlantic Ridge. The box indicates the limits of the maps in Figures 2–4. CAMH is the central anomaly magnetic high along the axis of the rift valley. Principal magnetic anomalies are identified off axis, and nontransform discontinuities are shown by bold lines.

edge of the rift valley floor. In these locations the hanging wall consists of crust composing the valley floor.

On the basis of locations of interpreted breakaways and terminations at megamullions and observed crustal ages at these locations, slip on individual detachment faults in the North Atlantic persists for ~1.0–2.6 m.y. [*Tucholke et al*., 1998]. With these slip durations the megamullion footwalls could exhume substantial sections of lower oceanic crust and possibly even upper mantle. Few megamullions have been sampled, but rocks recovered by dredge and submersible to date invariably include gabbros and/or serpentinized peridotites, usually together with basaltic debris [*Auzende et al*., 1994; *Cannat et al*., 1995; *Cann et al*., 1997; *Karson*, 1999]. Overall, footwall rocks in megamullions have higher density than OC and segment-center crust, as indicated by residual mantle Bouguer gravity anomalies (RMBA) that are elevated by up to 20–25 mGal [*Tucholke et al*., 1998]. Gravity modeling of one megamullion near Atlantis Fracture Zone on the Mid-Atlantic Ridge suggests mantle exposure toward the termination [*Blackman et al*., 1998], and this has been confirmed by mantle velocities observed in near-bottom seismic experiments [*Collins and Detrick*, 1998].

Because of their geological characteristics and apparent mode of origin, megamullions offer excellent opportunities to study deep sections of the crust and the upper mantle, to investigate processes of fault nucleation, evolution, and strain localization, and thereby to constrain fundamental tectonic patterns in ocean crust. Furthermore, there is a strong analogy between oceanic megamullions and continental metamorphic core complexes [e.g., *Howard and John*, 1987; *Davis and Lister*, 1988]. Both sets of features appear to originate by detachment

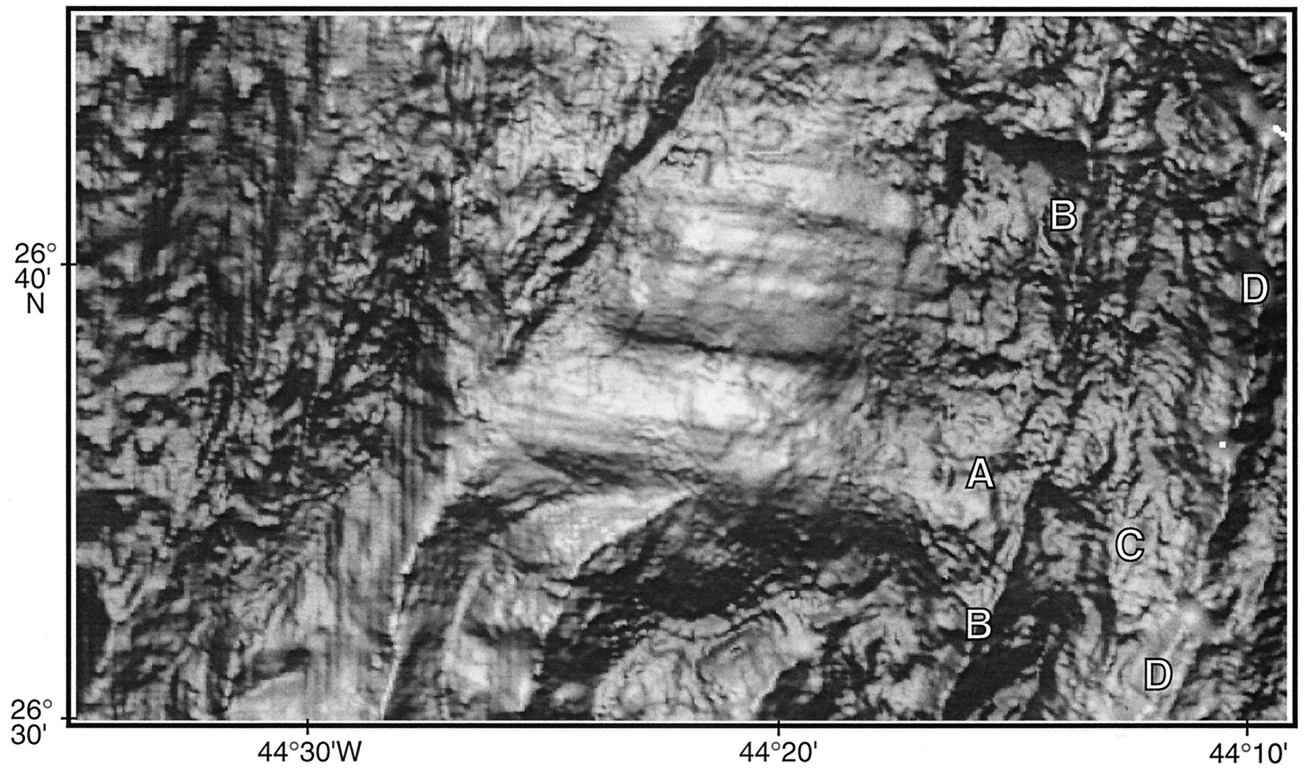

Figure 2. Shaded relief bathymetry of Dante's Domes megamullion on the east flank of the Mid-Atlantic Ridge near 26°35′N. The map is constructed from Hydrosweep multibeam bathymetry gridded at 100-m intervals and illuminated from the north. The neovolcanic zone in the axis of the rift valley is at the upper left. The domed structure at center is interpreted to be the footwall of a long-lived detachment fault. Its surface is corrugated by ~E-W flow line parallel structures with amplitudes less than a few tens of meters, and these are interpreted to be fault mullions; ship tracks were oriented NW-SE, so it is clear that the mullions are not beam-point artifacts. Letters A–D locate ridges identified in Figure 3 and discussed in the text. For additional structural interpretations including fault breakaway and termination, see Figure 3.

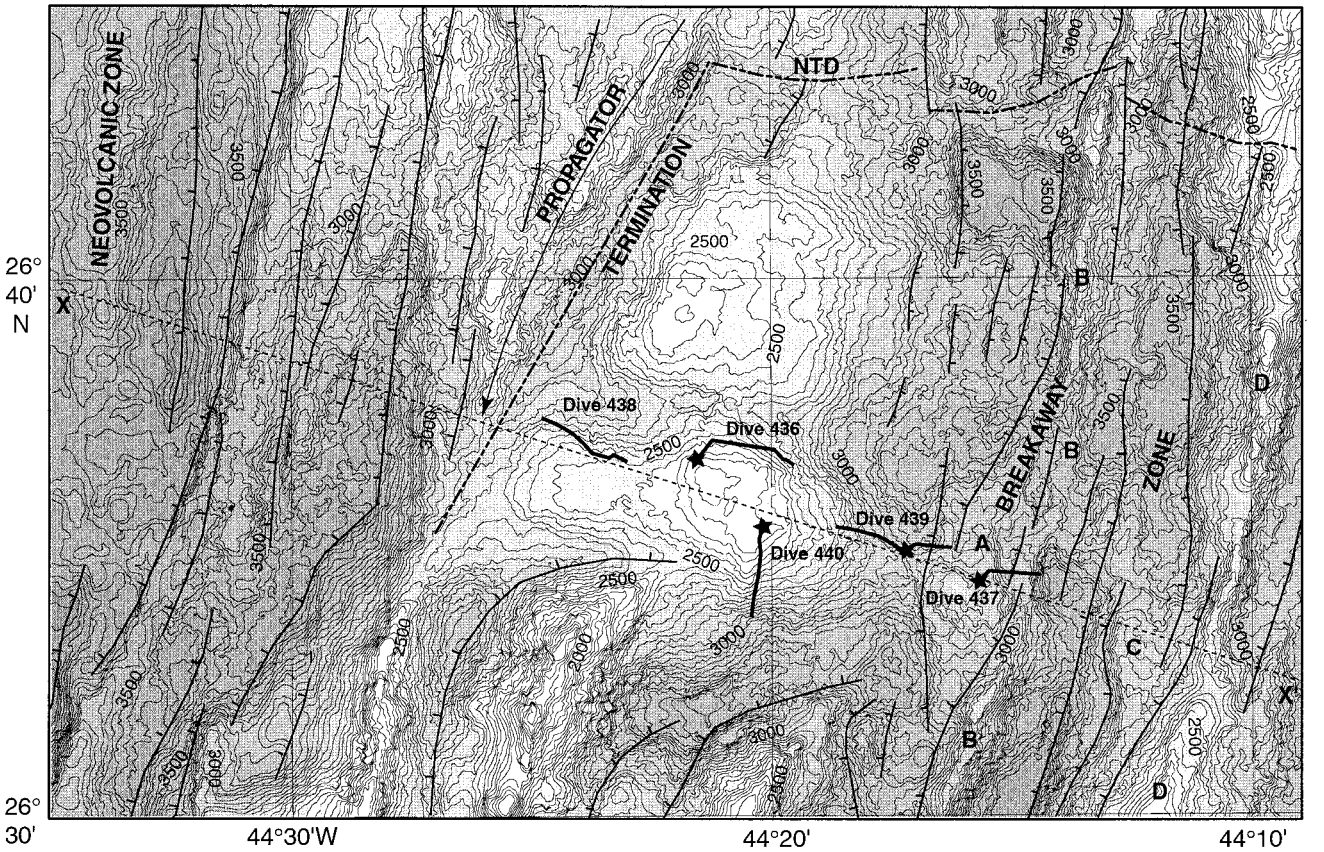

Figure 3. Multibeam bathymetric map of Dante's Domes megamullion with simplified structural interpretation. The map is from Hydrosweep multibeam bathymetry gridded at 100-m intervals, and contour interval is 50 m. Normal faults are indicated by lines with ticks on the hanging wall. NTD is a small, nontransform discontinuity. Tracks of five dives of *Shinkai 6500* are indicated as bold solid lines, with stars showing locations of on-bottom gravity and heat flow measurements. The thin dashed line from X to X′ shows the cross section represented in Figures 9 and 11.

faulting; they generally have similar scales (~10–40 km diameter), "turtleback" shapes, and development of fault mullions, and they exhume rocks from depths of several kilometers and greater. Comparison of the oceanic and continental features should ultimately yield new insights into lithospheric tectonism in both environments.

To begin testing interpretations of megamullions, which thus far are based mostly on surface ship geophysical data and scattered dredge results, we conducted the first submersible dive program designed to investigate one of these features systematically. We chose a well-developed megamullion, here termed Dante's Domes, on the Mid-Atlantic Ridge near 26°35′N (Figures 1–3). Five dives observed and sampled the feature from the apparent breakaway zone to near the termination. Our results are consistent with the interpretation that the megamullion originated by long-lived detachment faulting. They also offer new insights into tectonic patterns of megamullion development and possible relations of that development to long-term patterns in cyclicity of magmatism at the Mid-Atlantic Ridge.

2. Geological Setting of Dante's Domes

Dante's Domes is located in the rift mountains just east of the Mid-Atlantic Ridge axis (Figures 1–3) in crust with a mean spreading half rate of 9 km m.y.$^{-1}$ [*Tivey and Tucholke*, 1998]. At its northern margin it is bounded by a minor right stepping discontinuity that has an age offset ranging from near zero to no more than a few hundred thousand years. Immediately south of the megamullion, a series of isochron-parallel abyssal hills curve sharply eastward and die out at its southern edge. Each of these ridges was formed by a separate normal fault. The ridge curvature indicates that another right stepping discontinuity may be present along the southern edge of the megamullion, although no magnetic anomaly offset has been identified there. This discontinuity or transfer zone separates regions with very different styles of tectonic extension to the north and south, but it is uncertain how this is accomplished kinematically.

The eastern limit of the megamullion appears to coincide with a set of ridges between magnetic anomalies 2 and 2A in ~2.0–2.8 Ma crust. According to the detachment fault hypothesis the fault nucleated within this breakaway zone. To the west the megamullion terminates along a NNE trending valley on the young side of anomaly 1r, and a prominent ridge parallels the valley on its west side. The valley and ridge are oblique both to magnetic anomalies and to the regional trend of abyssal hills, which are oriented in a more northerly direction. The oblique ridge's position and orientation suggest that termination of megamullion growth was caused by a southward propagating rift from ~1.3 Ma to 0.7 Ma. Thus the megamullion

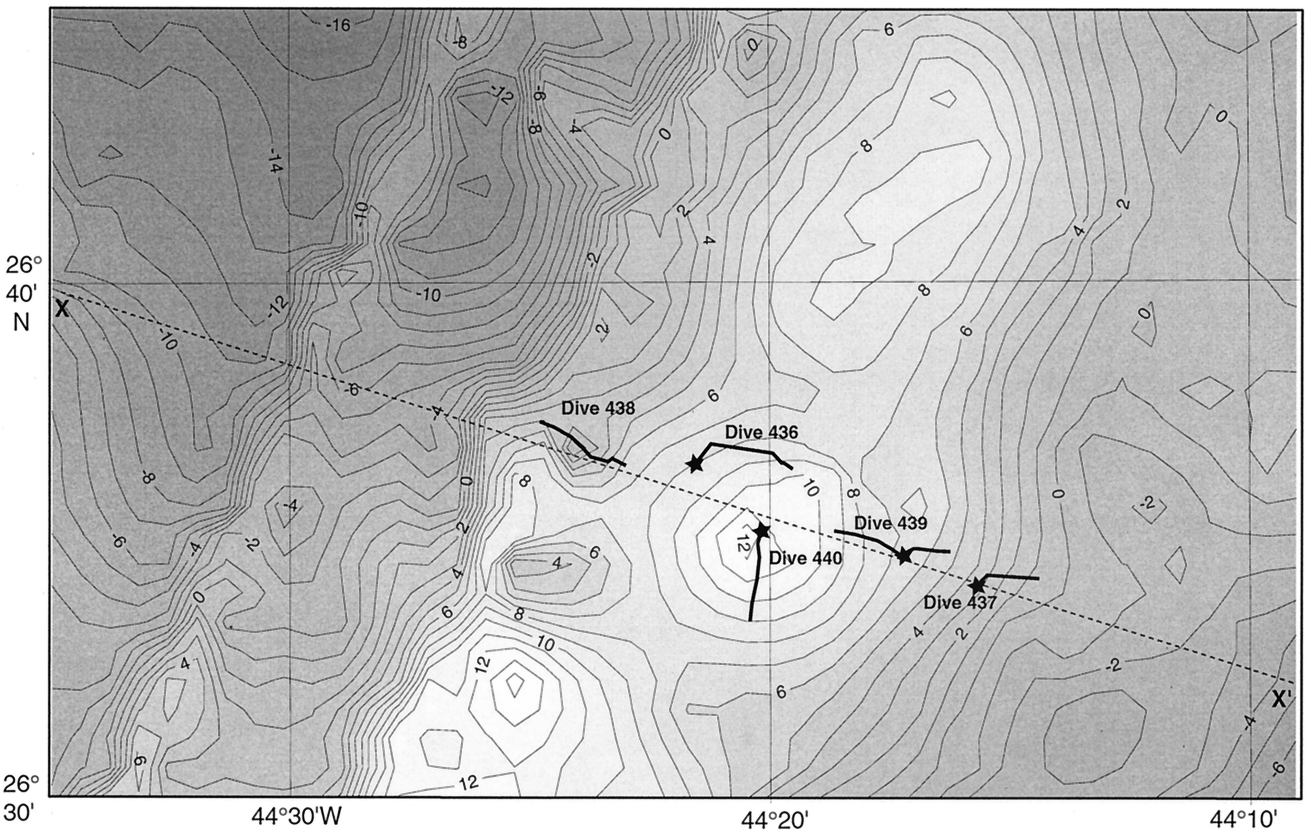

Figure 4. Map of residual mantle Bouguer gravity at Dante's Domes megamullion (J. Lin et al., unpublished manuscript, 2000). Contour interval is 1 mGal. Note the broad, NNE trending isochron-parallel gravity high centered on the megamullion in the area of dive 440; gravity values along this high are 18–28 mGal higher than over younger and older crust. The pair of small, NNE trending gravity "ridges" in the left part of the map are artifacts from edge matching of multibeam bathymetry; they do not affect the longer wavelengths in the gravity data which we model in Figure 9, and thus they are ignored in Figure 9. *Shinkai 6500* dive tracks and gravity/heat flow stations are as shown in Figure 3.

developed over a total period exceeding a million years. On average, the extent of the megamullion surface from breakaway to termination is about 18 km.

The megamullion consists of two broad domes lying side by side along the strike of isochrons. Compared with normal ocean crust, both domes have exceptionally smooth surfaces, as indicated in sea surface multibeam bathymetry (Figures 2 and 3). However, the surfaces are covered by small-amplitude (tens of meters) corrugations, many of which extend >10 km in the spreading direction. The corrugations resemble mullion structures commonly developed on fault surfaces. They are poorly developed (or preserved) in the first ~5 km west of the breakaway zone, but they are distinct on the younger, domed surfaces right up to the termination. Within ~5 km of the breakaway zone, small (up to ~100 m), mostly east facing isochron-parallel scarps cross the surface of the megamullion. Over the younger surface of the domes much smaller isochron-parallel offsets (less than a few tens of meters) are present, as indicated by artificial low-angle illumination of multibeam bathymetry (Figure 2).

Dante's Domes exhibits an RMBA gravity maximum that is centrally located between the breakaway and termination (Figure 4). This gravity high is up to 20–25 mGal higher than gravity over younger or older crust and suggests crust that is ~2 km thinner. Owing to uncertainties in density associated with serpentinization, the value of 2 km may be a minimum thickness reduction. *Minshull* [1996] compared along-axis gravity and seismic estimates of crustal thickness in slow spreading crust and found that the gravity data underestimate crustal thickness variations. The discrepancy may result from density reduction caused by serpentinization in the upper mantle.

Magnetic anomalies 1r through 2 are identifiable over the megamullion, but they have lower amplitude than anomalies in surrounding crust. Magnetization contrasts in the upper, extrusive crust are normally considered to be responsible for generating magnetic anomalies [*Talwani et al*., 1971; *Harrison*, 1987; *Tivey*, 1996], but at slow spreading ridges much of the magnetization may reside within the subvolcanic lithosphere [e.g., *Tivey and Tucholke*, 1998]. The low anomaly amplitude over the megamullion could indicate that one or both of these layers is thin compared with surrounding crust.

3. Submersible Data Acquisition and Processing

Five dives, each traversing 2–4 km of seafloor, were conducted across the southern dome of Dante's Domes using the Japanese submersible *Shinkai 6500* (Figures 3 and 4). Four dives (436–439) were aligned along a transect extending from the breakaway zone to near the termination, and a fifth dive (440) was centered on the RMBA high near the middle of the

dome. To optimize our chances of observing basement outcrops, all dives were located in areas where previously acquired Hawaii Institute of Geophysics and Planetology (HIGP) Acoustic Wide-Angle Imaging Instrument, Mapping Researcher 1 (HAWAII MR1) long-range side-scan sonar records showed maximum backscatter from the seafloor.

Seafloor depth profiles along the dive tracks were generated by summing submersible pressure-depth and altimeter records. Visual observations were made directly through the submersible's viewing ports and were recorded on one external 35-mm film camera and two video cameras (one fixed and one pan and tilt). Eighty-one rocks were sampled using the submersible's manipulators.

On-bottom gravity measurements were made at one location during each dive except dive 438 (Figures 3 and 4). At each location the submersible was set on the seafloor, three repeat measurements were made using a LaCoste & Romberg G-1039 gravimeter, and a final value was calculated as the average of the repeat measurements. The free-water anomaly was calculated by correcting for different seafloor depth at each measurement location (i.e., free-water correction, with a vertical gravity gradient value in seawater of 0.22242 mGal m^{-1} assumed) and for the shape of the Earth (latitude correction). The mantle Bouguer anomaly was calculated by removing from the free-water anomaly the gravitational attraction of seawater and crust of assumed 6-km constant thickness; densities used for this calculation were 1030 kg m^{-3} for seawater, 2700 kg m^{-3} for the upper 2 km and 2900 kg m^{-3} for the lower 4 km of crust, and 3300 kg m^{-3} for mantle. This was done in a manner similar to terrain corrections for land gravity survey [e.g., *Hammer*, 1939]: A circular area with a 16-km radius around each measurement location was divided into compartments by annular rings and radial lines; the mean seafloor depth for each compartment was calculated from multibeam bathymetry (100-m grid cell size); and the gravity effects of seawater and crust in all compartments were calculated. It was assumed that the seafloor and the other two interfaces outside this circular area are at the same depths as they are at the measurement location. Finally, we calculated a residual mantle Bouguer anomaly by removing lithospheric cooling effects based on a three-dimensional passive upwelling model [e.g., *Kuo and Forsyth*, 1988].

The seafloor gravity results were compared with sea surface gravity obtained during a prior cruise (track spacing of 5 km and crossover errors <1 mGal (J. Lin et al., unpublished manuscript, 2000) (Figure 4). For the sea surface data, free-air gravity anomaly had been calculated by making Eötvös and latitude corrections. Mantle Bouguer anomaly was calculated assuming 6-km-thick crust, as for the seafloor data, but with the entire crust having 2700 kg m^{-3} density. Residual mantle Bouguer anomaly was computed by removing lithospheric cooling effects, as already noted. A fast Fourier transform method [*Parker*, 1972] was used in the calculation of the mantle Bouguer anomaly, and, as a result, the zero level for this anomaly and the residual mantle Bouguer anomaly is arbitrary. For the seafloor data a constant was subtracted from the residual mantle Bouguer anomalies to approximately match the mean theoretical gravity values obtained from the models. Mean seafloor and sea surface residual gravity data were plotted and modeled together (see Figure 9). Any offset between the two data sets should be small (probably less than a few milli-Gals), but the value is unknown because of the arbitrariness in zero level of the sea surface data.

An *Alvin*-type thermal probe and resistance heater [*Becker and Von Herzen*, 1996] were used to measure in situ thermal profiles and thermal conductivity, respectively, in the same locations as the gravity measurements. The 0.6-m-long probe has five thermistors mounted at 10-cm intervals beginning 11.5 cm from the probe tip. The probe was inserted into the sediment by *Shinkai*'s manipulator and kept stationary for 20 min (10 min recording of equilibration toward the in situ temperature gradient and 10 min recording of thermal decay following the introduction of a calibrated heat pulse). In situ temperatures were calculated by extrapolating measured temperatures to infinite time in order to remove the effect of frictional heating caused by probe penetration. Thermal conductivity was measured using the pulse-probe method [e.g., *Davis*, 1988].

4. Dive Observations

Taken together, the five *Shinkai 6500* dives constitute nearly a complete transect of the southern dome of Dante's Domes megamullion in the direction of plate flow lines. We summarize here our direct seafloor observations beginning in the area of the interpreted breakaway zone and extending toward the megamullion termination (Figure 3).

4.1. Dive 437

Dive 437 started in a sedimented valley at the base of a large, north-south-elongated ridge in the breakaway zone (ridge B in Figure 3), and it traversed west and southwest to the crest of juxtaposed ridge A (Figure 5a). The average slope along the first one third of the traverse dips ~30° to the east, although local slopes reach 50°–60° over track distances of up to ~100 m. Gentler slopes were sedimented with calcareous pteropod ooze. Rock outcrops predominate on the steep slopes and consist of in-place basalt pillows, basalt talus, and marlstone with iron-manganese coating. The pillow basalt lobes are generally subequant (Figure 6a) and show no preferred flow direction (e.g., downslope). No faults or shear zones were identified, but they could be present beneath rubble and sediment cover. The observations of pillow basalt morphology and distribution suggest that the surface formed by volcanic deposition on horizontal to subhorizontal seafloor and that it subsequently acquired its slope by eastward tilting.

Toward the midpoint of the dive, the submersible crossed two 70- to 80-m-high ridges. The eastern face of the east ridge is a continuation of the pillow lava slope just discussed, and the eastern face of the west ridge was covered with basaltic talus. The western faces of both ridges are steep, ranging from 40° to 70°, and were not observed visually because they fell away sharply from the submersible trajectory. The gentler east facing slope along the remainder of the dive track (average of ~10°, locally up to 50°) is mostly sediment-covered, but it shows local outcrops of in-place pillow basalts and scattered basaltic debris. Eleven rock samples were taken along the dive traverse, and they consist of pillow lavas with glassy palagonite rims, fine-grained basalts, and marlstones.

4.2. Dive 439

Dive 439 traversed west from the breakaway zone and across a bathymetric saddle onto the lower flank of the megamullion dome (Figure 5b). The first part of the dive crossed a ridge ~100 m high. The east facing slope of the ridge dips ~10°–20°; it is mostly sediment-covered but shows scattered fragments of

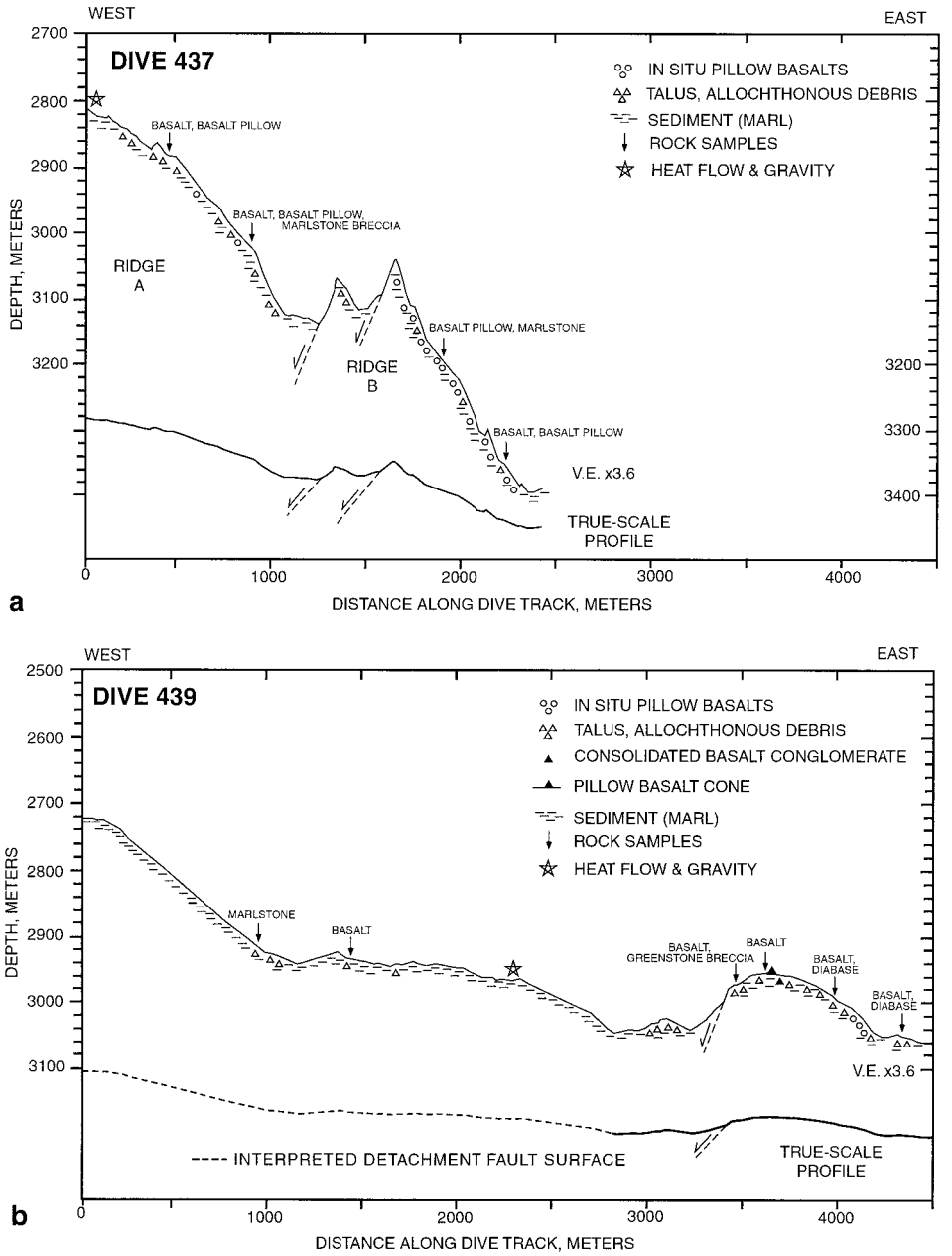

Figure 5. Summary of geological results for traverses of (a) dive 437 and (b) dive 439. Indicated lithology and structure are interpreted from visual observations and recovered rocks; sample locations are shown by arrows. The interpreted detachment fault surface in subvolcanic lithosphere is shown by a dashed line in the true-scale profile at the bottom of Figure 5b. Stars mark locations of gravity and heat flow measurements. Note that because of variable azimuths of the submersible track, slope dips and inflections here and in Figures 7 and 8 do not necessarily reflect true cross-sectional topography.

basalt and basalt-claystone breccia. In-place pillow basalts occur near the base of the slope, and a small pillow basalt cone ~3 m high was observed at the ridge crest. Both observations suggest that the slope is at least partially a volcanic depositional surface. The west flank of the ridge fell away from the submersible trajectory and was not observed visually, but it dips as steeply as ~45°.

Over the remainder of the dive track the submersible traversed over the saddle and onto the lower part of the main dome. Here the seafloor is very smooth and sediment-covered, with <10° east to northeast dipping slopes. The only interruptions are created by local patches of loose basaltic debris. Actual sediment thickness is uncertain. A sediment veneer less than a few meters thick overlying strongly reflective basement is suggested locally in shipboard 3.5-kHz profiles in this area and over the dome to the west, but this veneer is difficult to resolve among side echoes. At the heat flow stations on this and other dives the 0.6-m probe was inserted without encountering hard rock.

Eleven rock samples were recovered during dive 439. They consisted of seven pillow basalts in varying states of alteration, some with palagonitic rims; one greenstone breccia; two coarsely crystalline basalts or diabases; and one manganese-encrusted marlstone.

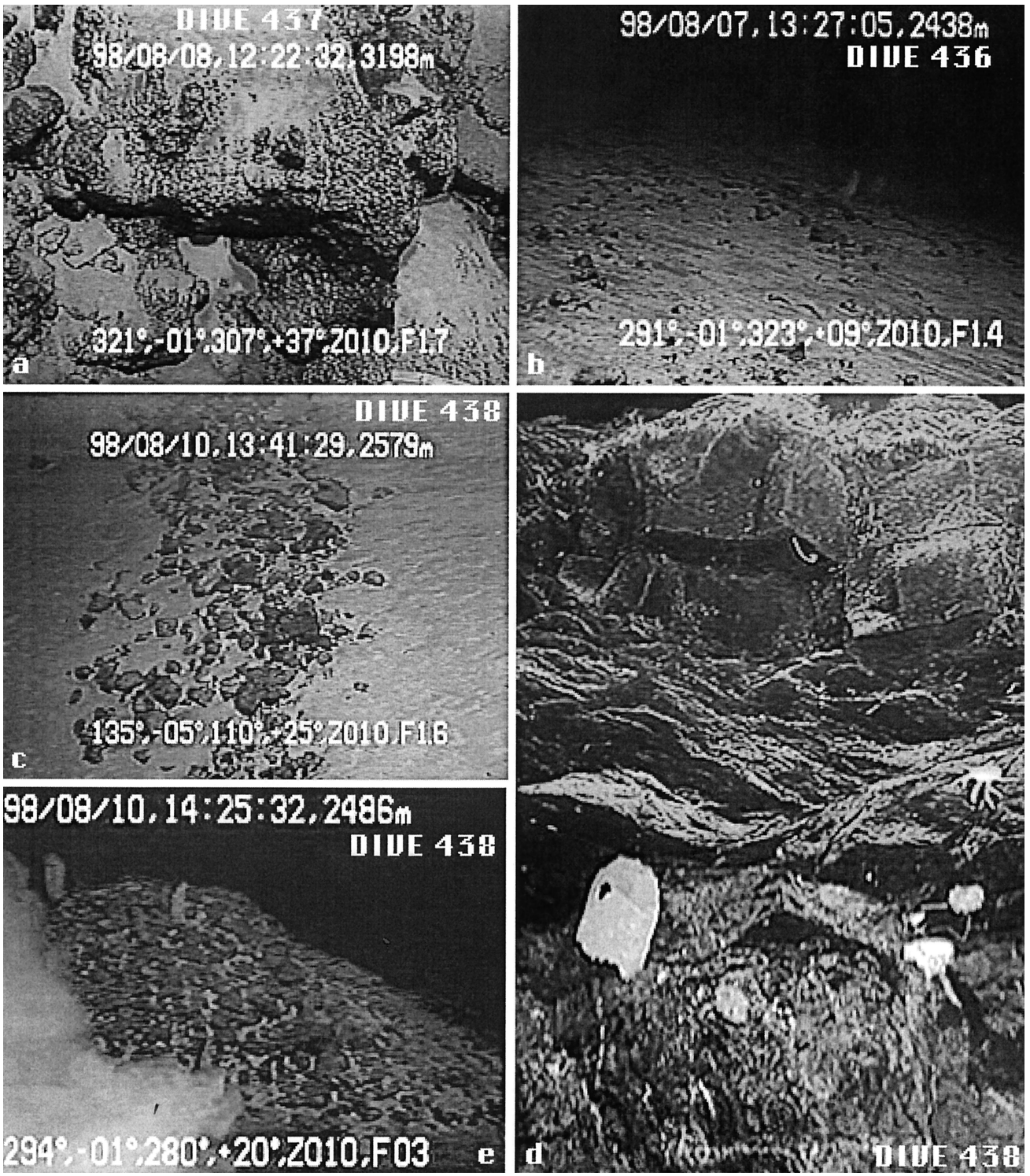

Figure 6. (a) Video image of pillow basalts on steep east facing slope traversed in the first part of dive 437. Image width is ~2 m. (b) Gently northward sloping surface of the megamullion dome observed during dive 436. This kind of flat, rippled, sediment-covered surface with scattered basaltic debris is characteristic of the megamullion dome for >13 km in the spreading direction. Image width is ~6 m in the near field. (c) "Fence" of displaced basaltic debris that sinuously follows bathymetric contours along the flank of the megamullion dome (dive 438). Image width is ~6 m in the near field. (d) Video frames mosaicked to show small, east facing fault scarp that exposes (bottom to top) jointed basalts, shear zone consisting of greenstone, and a capping basalt flow (dive 438). Image width is ~1 m. (e) Isolated pillow basalt cone ~3 m high and 10 m in diameter sitting atop detachment surface (dive 438). Digital data displayed at tops of frames are date, time, and submersible depth; displayed at bottoms of frames are submersible heading, submersible inclination (negative is up), true camera heading, camera inclination (positive is up), focal distance, and an object distance.

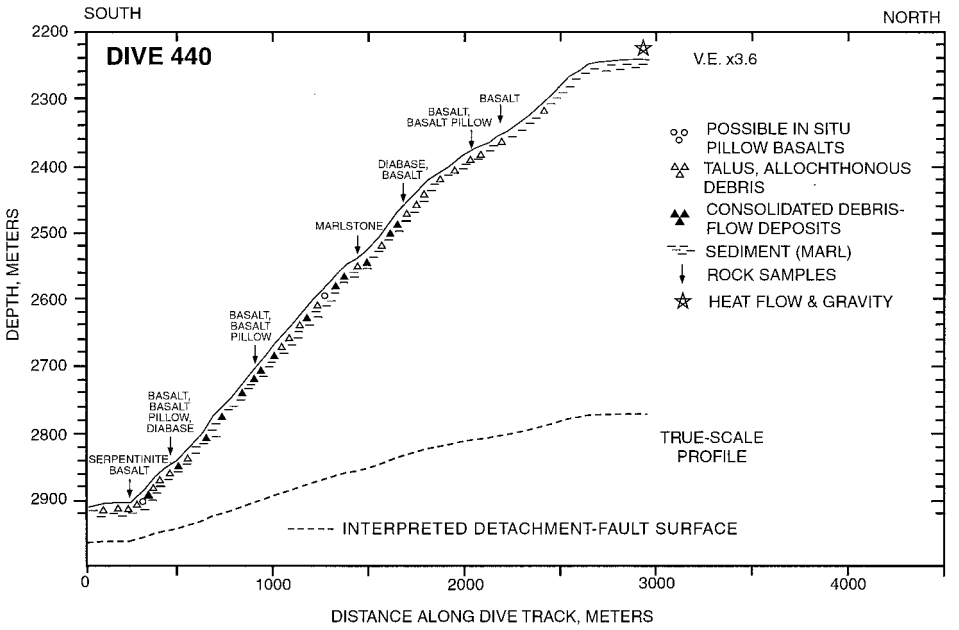

Figure 7. Summary of geological results for traverse of dive 440. See Figure 5 for explanation.

4.3. Dive 440

Dive 440 was located south of the main east-west transect on the southern part of the megamullion dome (Figures 3 and 7). It followed the axis of the maximum RMBA gravity anomaly and ended at the peak RMBA anomaly on the southern crest of the dome (Figure 4). The dive traversed the east slope of a spur that exhibits relatively steep dip and high backscatter in HAWAII MR1 long-range side-scan sonar records. Dive observations show that the slope is formed by a combination of gently dipping, sedimented ramps interspersed with steeply dipping (>40°) slopes laden with basaltic debris. Except for rare occurrences of possible in-place pillow basalts all observed and sampled rocks are talus. The seafloor near the top of the dome is very flat, gently sloping, and completely sediment-covered.

Thirty-one rock samples taken along the slope consist of aphyric to moderately crystalline basalts, pillow lavas, manganese-coated marlstones, and basalt-marlstone breccias. Two strongly sheared serpentinites were recovered in talus from the base of the slope near the beginning of the dive. Notably, in five dives on the megamullion these serpentinite samples from the RMBA gravity high were the only clearly subvolcanic rocks recovered. The altered ultramafic rocks exhibit microstructures indicative of deformation under hydrothermal conditions. Sample 440-1 is a mesh-textured serpentinite that is overprinted by both intact and sheared veins of chlorite ± amphibole. The mesh texture suggests that the initial alteration occurred under static conditions. The chlorite and amphibole grains are strongly aligned parallel to the orientation of the sheared veins. Sample 440-4 is a strongly foliated clay-rich schist. The foliation, defined by a preferred orientation of phyllosilicate grains, is often kinked. Textural relations indicate that clay replaced serpentine ± chlorite. Relict islands of serpentine are also strongly foliated. No primary mineral phases were observed in either rock.

4.4. Dive 436

The northern margin of the megamullion dome was traversed from east to west during dive 436 (Figures 3 and 8a). The smooth appearance of the dome in multibeam bathymetry (Figures 2 and 3) was confirmed during this dive, which showed that the seafloor is exceptionally flat and that it dips gently northward at 10°–15° away from the dome crest (Figure 6b). The flat seafloor is completely covered by pteropod ooze. Basaltic debris is scattered across the surface, either partially buried or sitting on the sediment. We did not observe any rocks that could be identified as in place. The scattered rocks sometimes occur in clusters or in elongated "fences." The fences consist of straight to sinuous ridges of debris, 1–2 m high and up to several meters wide, which commonly trend parallel or subparallel to the bathymetric contours for distances of tens of meters to more than 100 m (Figure 6c). We crossed several gentle, isochron-parallel undulations on the dome surface (hundreds of meters in wavelength and tens of meters in amplitude) but no isochron-parallel scarps. The undulations may account for small isochron-parallel seafloor perturbations that appear in simulated low-angle lighting of multibeam bathymetry (Figure 2).

Eleven rock samples were recovered from the scattered debris on the dome surface. They included seven pillow basalts, three coarsely crystalline basalts or diabases, and an unusual sandstone consisting of angular quartz grains and minor plagioclase cemented by a carbonate matrix.

4.5. Dive 438

The youngest part of the megamullion dome was traversed from west to east during dive 438 (Figures 3 and 8b). As in dive 436, the dome surface was remarkably flat, sediment-covered, and gently sloping to the north, with occasional long-wavelength, isochron-parallel undulations. Basaltic debris was commonly observed in fences and clusters and was randomly

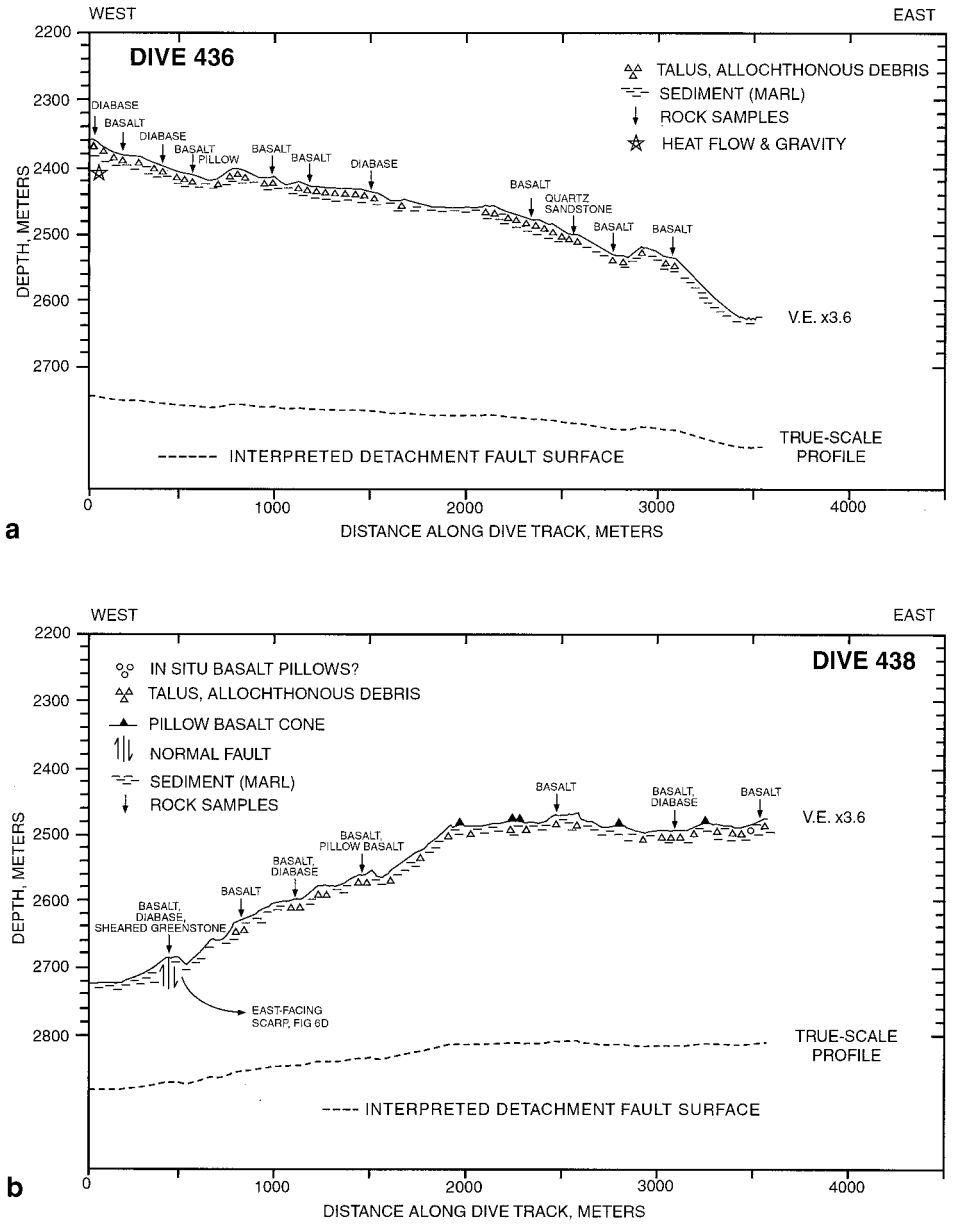

Figure 8. Summary of geological results for traverses of (a) dive 436 and (b) dive 438. See Figure 5 for explanation.

scattered across the seafloor. Unlike dive 436, however, two kinds of in-place basement exposures were observed. The first, near the beginning of the dive, was a vertical, ~3-m-high, east facing scarp formed by a normal fault. The scarp exposes three units (Figure 6d). At the base is a 2-m-thick section of vertically jointed basalts; these may have been emplaced as a thick flow or sill, but they could also be dikes. The top of these basalts is abruptly truncated by a horizontal shear zone ~0.5 m thick that consists of intensely deformed greenstone (amphibole + chlorite). The shear zone is capped unconformably by a thin (~0.5 m) basalt flow that is vertically jointed and has a lobate pillowed surface covered by a few tens of centimeters of sediment.

The second kind of in-place exposure consists of small volcanic cones observed in the eastern half of the dive above ~2500 m depth. The cones protrude above the otherwise monotonously flat seafloor (Figure 6e), and they normally are 1 m to several meters high and 5–20 m in diameter. They are composed of intact pillow lavas that have individual lobes typically tens of centimeters in diameter. One small exposure of possibly in-place pillow basalts not forming a cone was also observed near the end of the dive. Fifteen rocks sampled during the dive consisted of basalts, plus greenstones recovered from the shear zone noted above.

4.6. Gravity

Seafloor gravity measurements reduced to residual mantle Bouguer anomaly are shown in Figure 9. The highest gravity value was observed on dive 439 on the eastern, older edge of the main dome, and a value 5 mGal lower was observed near the crest of the dome on dive 440. Significantly lower values appear near the breakaway on dive 437 and west of the main

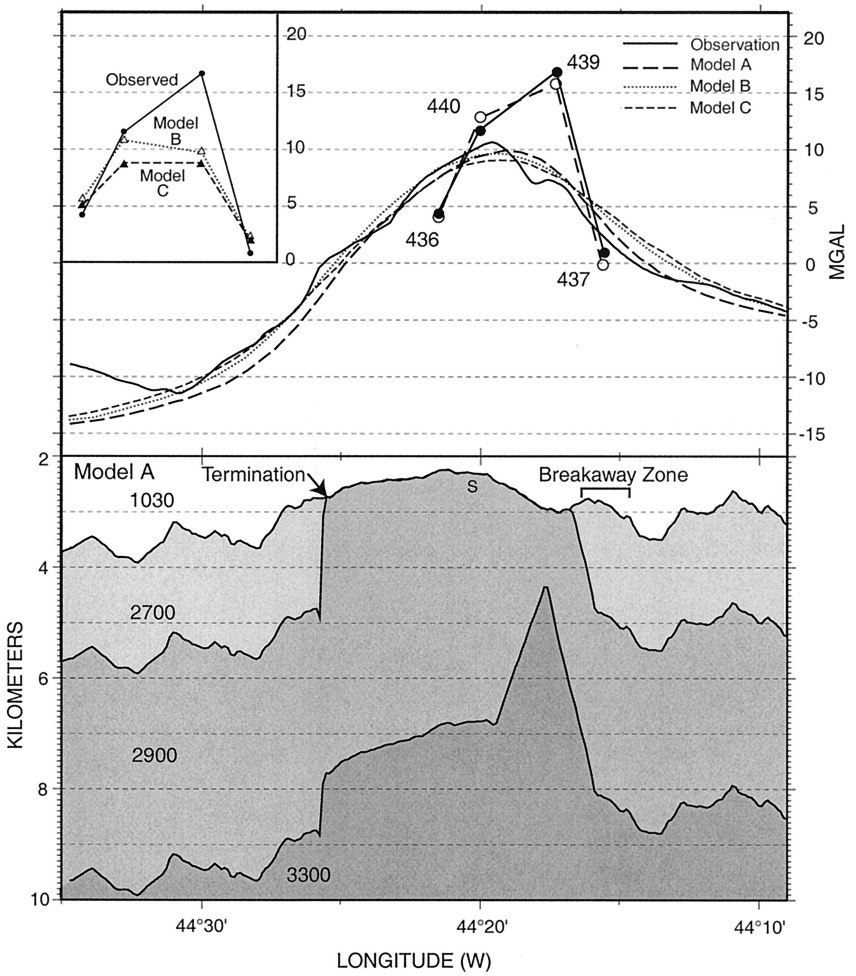

Figure 9. Gravity observations and models for transect X–X′ in Figure 3. (top) Residual mantle Bouguer anomaly (RMBA) from shipboard gravity data (solid curve) and from individual seafloor measurements (solid circles denoting the dive and connected by solid lines, projected onto the transect), together with modeled RMBA at sea surface and at seafloor. For clarity, the result of model A for seafloor gravity is shown in the large plot, and results of models B and C summarized in the text are shown separately in the inset at left. (bottom) Density distribution used to calculate sea surface and seafloor gravity in model A in top plot. Three layers with densities of 2700 kg m^{-3} (basalt), 2900 kg m^{-3} (e.g., gabbro, serpentinized peridotite, and possible intrusives), and 3300 kg m^{-3} (peridotite) are assumed to lie below seawater (1030 kg m^{-3}). The long-wavelength sea surface gravity anomaly is explained by intermediate densities beneath most of the megamullion dome, while the short-wavelength anomaly observed at the sea floor also requires a narrow, high-density zone beneath the older, eastern margin of the dome. The S near 42°20′W indicates the location where serpentinites were sampled on dive 440.

dome on dive 436. The elevated gravity values, particularly from dive 439, document short-wavelength anomalies of high-density lithosphere beneath the central to eastern part of the megamullion dome that cannot be observed in sea surface gravity. Further implications of the gravity measurements are discussed in section 5.1.

4.7. Heat Flow

To analyze the heat flow data, we first considered the effect of thermal conductivity variation versus depth [*Bullard*, 1939]. Under a conductive regime a plot of temperature versus thermal resistance (an integration of the inverse of thermal conductivity) should be linear. In such "Bullard plots" (Figure 10a) the heat flow value can be obtained directly from the slope of the best linear fit to the data (Q_{cond} in Table 1). For the easternmost dive (437) near the breakaway the profile is linear within the error, whereas for the western dives that reach onto the megamullion dome (439, 440, and 436) the profiles are convex upward.

The cause of the convex profiles could be either a time-dependent reduction in bottom water temperatures or an upward flow of fluid within the sediment. If the cause was a change in bottom water temperature, we would expect either a similar effect at all measurement locations or an effect that varies systematically with seafloor depth. Instead, both the shallowest (436 and 440) and deepest (439) measurements show curved profiles, whereas the dive 437 measurement at an intermediate depth is linear within measurement error (Figure 10a).

From these observations the simplest explanation of the convex profiles is that they reflect upward fluid flow within the sediments. If we assume one-dimensional, vertical pore fluid

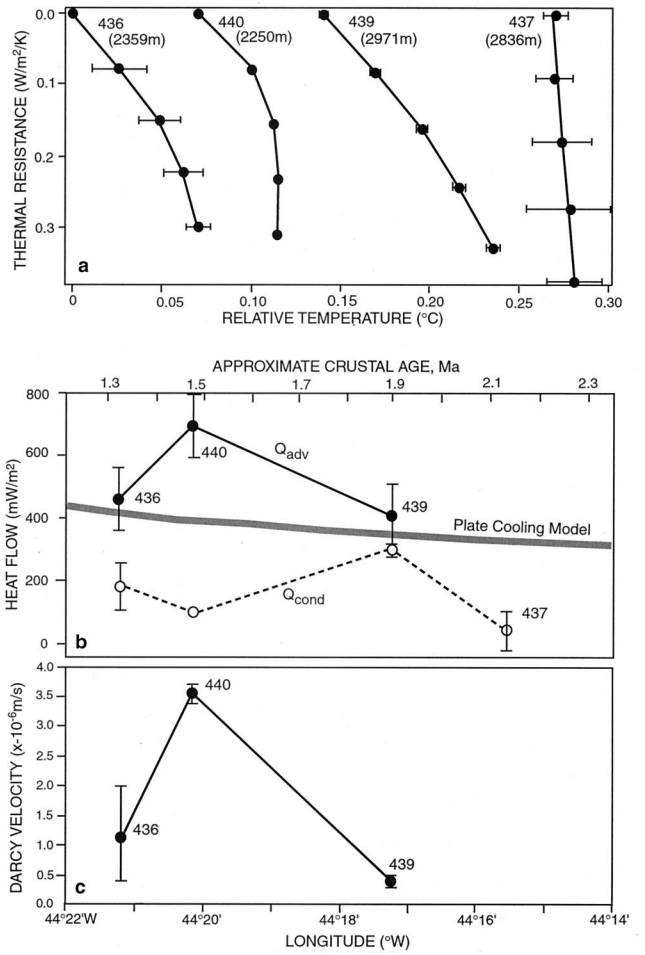

Figure 10. Results of heat flow measurements at Dante's Domes megamullion, arranged from near the breakaway (right) westward toward the termination. (a) Bullard plot of temperature versus integrated thermal resistance. Dive numbers and seafloor depths are labeled. The concave upward curves suggest upward fluid flow in the three measurements at left, whereas the linear gradient at dive 437 is representative of conductive heat flow. Standard deviations on dive 440 are smaller than the size of the symbols. (b) Total heat flow calculated by assuming that upward fluid flow explains the curved plots in Figure 10a at dives 436, 440, and 439 (solid circles; see text) and conductive heat flow calculated from linear best fits of the data in Figure 10a (open circles). (c) Estimated Darcian flow velocity needed to explain curved plots in Figure 10a (negative flow is upward).

flow, we can estimate a total heat flow and a Darcian flow velocity by applying a nonlinear fit to the data [*Bredehoeft and Papadopulos*, 1965]. These values, listed as Q_{adv} and V_d, respectively, in Table 1, are plotted in Figures 10b and 10c together with Q_{cond}. Total heat flow at dives 436 and 439 is approximately that expected for crust of this age in a plate-cooling model [*Parsons and Sclater*, 1977], while the value at dive 440 is significantly higher and that at dive 437 is significantly lower. It is possible that heat flow at dive 437 is depressed by downward fluid flow; however, we cannot be certain of this because marked curvature in the Bullard plot would be inverted and also deeper than our shallow measurements are likely to detect.

5. Interpretation and Discussion

5.1. Megamullion Dome

We interpret the remarkably flat seafloor that extends for >13 km from about the midpoint of dive 439 westward past the transect of dive 438 as the sedimented surface of a detachment fault that formed Dante's Domes megamullion (Figure 11). Although thin sediment cover masks nearly all of this surface from direct observation, it is clear that the smooth morphology was not created by extrusive volcanism. The fault interpretation is consistent with the surface ship bathymetric data that show corrugations interpreted as slip-parallel mullion structures (Figure 2) and is consistent with gravity data (Figures 4 and 9) and recovery of serpentinized peridotites that indicate exhumation of lithosphere having higher-than-normal density in the megamullion domes. Other seafloor observations, although they do not provide conclusive tests, are consistent with the detachment fault hypothesis, as outlined below.

Direct evidence for shearing that may be associated with the fault surface is limited to two examples. One is the sharply bounded, 0.5-m-thick zone of highly sheared greenstone exposed in the small scarp near the west end of dive 438 (Figures 6d and 8b). Along the strike of the scarp this shear zone parallels the seafloor, which we interpret to reflect the orientation of the detachment surface. Foliation in the outcrop and in recovered samples also indicates that the shear zone extends subhorizontally into the scarp face, so that it also parallels the seafloor in the dip direction. It is possible that this shear zone is the detachment fault itself, in which case the veneer of overlying basalts could have been deposited either as an onlapping flow within the rift valley or by off-axis volcanism. It seems unlikely that this zone is a secondary shear paralleling the detachment surface since it is so close to that surface.

The other evidence for shearing is the deformed serpentinite and strongly foliated clay-rich schist recovered during dive 440. These samples were recovered within talus, so the kinematic context of their deformation is unknown. They could have been deformed in the primary detachment fault or in other

Table 1. Results of Heat Flow Measurements on *Shinkai 6500* Dives[a]

Dive	Latitude, °N	Longitude, °W	G, m°K m^{-1}	K, W m^{-1} °K^{-1}	Q_{cond}, mW m^{-2}	Q_{adv}, mW m^{-2}	V_d, m s^{-1}
436	26°36.79′	44°21.20′	133	1.33	176 ± 73	450 ± 100	$-1.2 \pm 0.8 \times 10^{-6}$
437	26°34.41′	44°15.53′	41	1.04	42 ± 66	···	···
439	26°34.87′	44°17.25′	242	1.21	293 ± 27	405 ± 100	$-0.4 \pm 0.1 \times 10^{-6}$
440	26°35.23′	44°20.17′	78	1.28	100 ± 7	690 ± 100	$-3.6 \pm 0.2 \times 10^{-6}$

[a]G is temperature gradient, K is thermal conductivity, Q_{cond} is conductive heat flow determined from Bullard plot, Q_{adv} is heat flow with fluid flow considered (errors are estimates), and V_d is estimated fluid flow velocity (negative is upward).

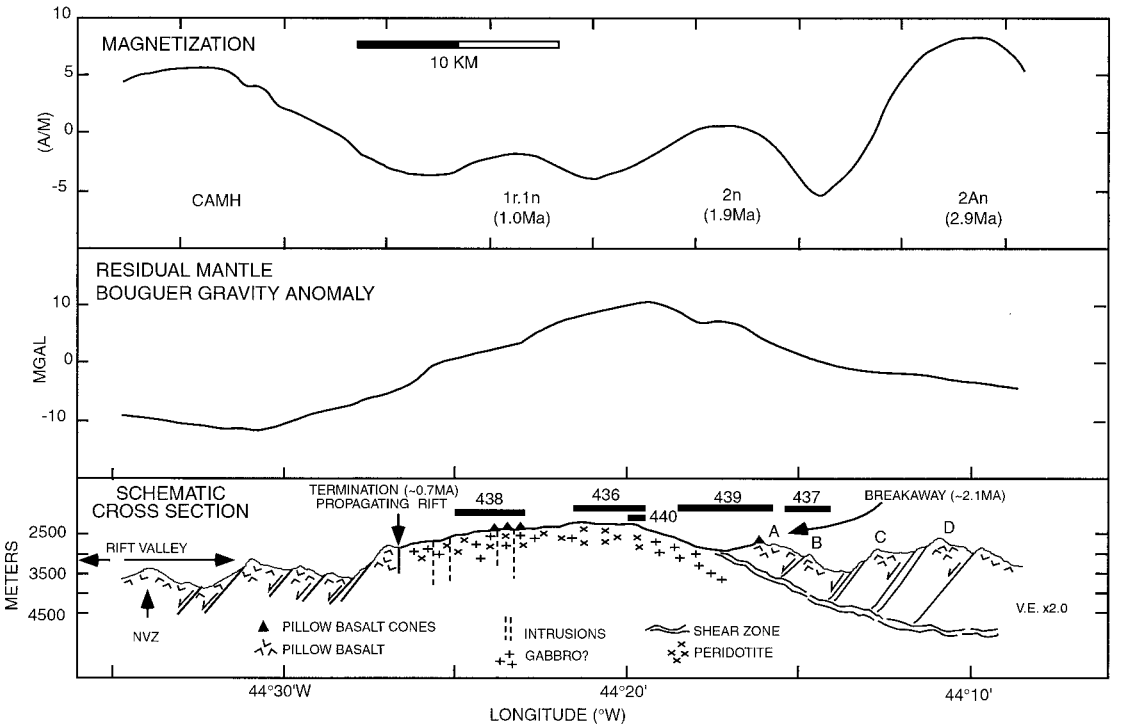

Figure 11. Cross section across Dante's Domes along X–X′ in Figures 3 and 4, showing magnetization and interpreted anomalies (ages in million years), residual mantle Bouguer gravity anomaly, and schematic interpretation of geologic structure. CAMH is the central anomaly magnetic high along the rift axis, and NVZ is the neovolcanic zone.

shear zones (e.g., small-throw, high-angle faults) that may have cut through the megamullion surface.

Long-lived detachment faulting should expose subvolcanic crust and possibly even upper mantle. The recovery of serpentinites at the position of the RMBA gravity high demonstrates that such rocks were exposed at Dante's Domes. It is unclear, however, what crustal or mantle rocks may be exhumed by the fault elsewhere on the megamullion. With the exception of the in-place basalts and volcanic cones observed on dive 438 (discussed below), none of the abundant basaltic and diabasic debris recovered across the dome can be shown to be locally derived, so it may not be representative of underlying footwall rocks. We suspect that most of this debris was clipped from the overlying hanging wall when the detachment fault was still active.

To help constrain the distribution of subsurface rock types within the footwall, we modeled the sea surface RMBA gravity in conjunction with the on-bottom gravity measurements (Figure 9). We did not attempt to model short-wavelength anomalies in the sea surface gravity but instead sought to replicate the long-wavelength (~20 km) gravity high that is characteristic of the megamullion. We did, however, include small-scale perturbations in density structure that are necessary to explain the on-bottom gravity measurements in conjunction with the sea surface data.

In model A (Figure 9), oceanic crust is assumed to be composed of a 2-km-thick 2700 kg m^{-3} basalt layer overlying a 4-km-thick 2900 kg m^{-3} "gabbro" layer west of the megamullion, while a slightly thinner (3.3 km thick) gabbro layer is used east of the breakaway zone. The thickness of the basalt layer decreases sharply westward from the breakaway zone, and the density structure changes abruptly farther to the west where a propagating rift is thought to have terminated megamullion formation. Over the central part of the dome the 2900 kg m^{-3} layer reaches the seafloor and is between 3.5 and 5.5 km thick. This layer may include gabbro, serpentinized peridotite, or both. Specific layer thickness and attitudes in this model, of course, are nonunique. Among many possible models, for example, the long-wavelength anomaly can be fit equally well by a model with 0.5 km of 2700 kg m^{-3} upper crust and total crustal thickness decreasing from ~4.5 to 3 km eastward from termination to breakaway (model B) or by a model with 1.5 km of 2700 kg m^{-3} upper crust and total crustal thickness decreasing from ~4 to 2.5 km eastward in this zone (model C) (Figure 9). Whatever the model, reduced crustal thickness beneath the megamullion dome is required to satisfy the gravity data. The simplest way to accomplish this is to thin or eliminate the low-density upper crust: The thinner this low-density lid is, the smaller will be the reduction in total crustal thickness that is required to fit the gravity observations.

The seafloor gravity observations provide further constraints. Model C (1.5-km-thick upper crust) provides a less satisfactory fit to seafloor observations than does model B (0.5-km upper crust) (Figure 9), which suggests that thin or missing upper crust is likely. Furthermore, to satisfy the on-bottom gravity measurement of dive 439, a narrow (~3 km) zone of high-density rock at shallow levels is required toward the eastern edge of the central dome (model A). The gravitational effect of this feature is largely indiscernable in the remote sea surface gravity data.

The combined gravity model and seafloor sample results suggest that lower crust, and possibly upper mantle, approaches or reaches the seafloor within a few kilometers west of the detachment fault breakaway as defined in section 5.2

(Figure 9). The serpentinized peridotites sampled during dive 440 occur a short distance farther west, within 6–7 km of the breakaway. Assuming that the crust in which the detachment fault formed was of normal, ~6-km thickness, these distances indicate that the fault initially dipped at least 45°, comparable to the dip of most seismogenic faults in ocean crust as indicated from teleseismic data [*Thatcher and Hill*, 1995]. If the fault nucleated in thinner crust, its dip could have been lower.

5.2. Breakaway Zone

The fault that sustained long-lived slip to form Dante's Domes probably nucleated at one of two breakaway locations. The first is a set of faults associated with the ridge at ~44°15′–44°17′W (ridge A in Figures 3 and 11), and the second is a fault set on the west side of the ridge located 8 km to the east (ridge B in Figures 3 and 11). Simulated low-angle lighting of multibeam bathymetry shows that mullion structures over the domes have some continuity eastward to ridge A but not beyond to ridge B (Figure 2). This observation suggests that ridge A should be considered the breakaway. However, dive 437 showed that the steep east face of ridge B, and possibly ridge A, is volcanic depositional seafloor that appears to have been rotated eastward by up to 50°–60°. It is unlikely that this large rotation can be explained solely by isostatic rebound of the rotating footwalls. Our preferred interpretation is that ridges A and B rotated above an older shear zone dipping west from the face of ridge C (Figure 11). In this configuration the older fault is considered to mark the breakaway, with ridges A and B constituting "rider blocks" atop the underlying detachment.

Actual structural relations probably are more complicated than suggested in this simple model. For example, ridges C and D, which in places also have steep east facing slopes compared with their west facing slopes (Figure 3), may also be rotated above a deeper, older shear zone still farther to the east. This pattern could be repeated well off axis, with successive faults soling into the same, but evolving, shear zone (Figure 11). In effect, the original "breakaway" could thus occur within much older crust, possibly even in the original, rifted continental margin. This becomes meaningless for understanding the development of mid-ocean megamullions. Thus we define the breakaway for an oceanic megamullion as the trace of the youngest fault responsible for exhumation of the megamullion. Following this criterion, the fault in ~2.2 Ma crust on the western side of ridge B constitutes the primary breakaway for most of Dante's Domes. Along our dive transect in the south a fault along the west face of ridge A in ~2.0–2.1 Ma crust probably constitutes a secondary breakaway (Figures 3 and 11); this fault trends into the ridge B fault to the north and south (Figure 3). Thus ridge A may be a rider block above the primary detachment.

5.3. Evolution of Dante's Domes Megamullion

Interpreted evolution of Dante's Domes megamullion is illustrated schematically in Figure 12. The breakaway of the fault that formed the megamullion is in ~2.0–2.2 Ma crust, and megamullion formation later terminated when a rift propagated southward along the rift valley between ~1.3 and 0.7 Ma. A primary feature of this model is that the megamullion footwall was exhumed by long-lived slip on a single detachment fault. Two observations support this idea. First, our dives traversed representative areas of the interpreted detachment for >13 km in the dip direction, and we found that it was characterized consistently by a single, smooth surface. Second, the

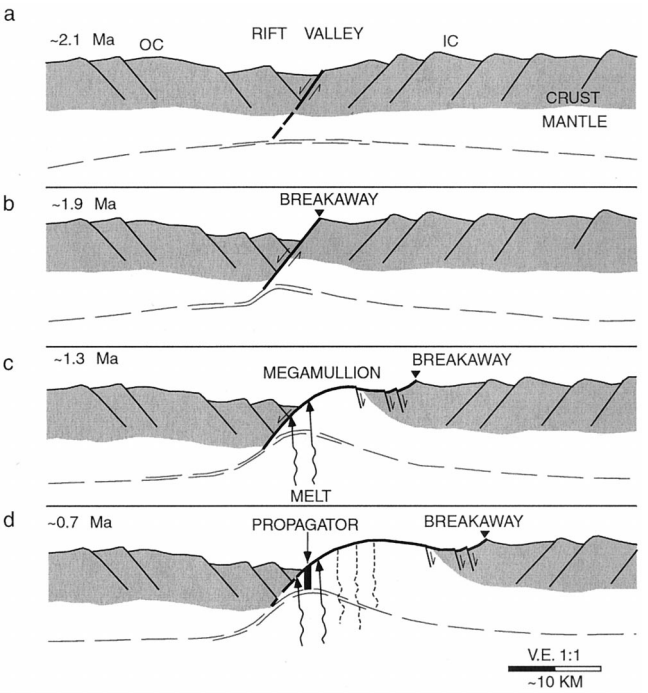

Figure 12. Schematic diagram showing proposed evolution of Dante's Domes megamullion. (a) Initial normal fault dipping ~45° through the crust to the brittle-plastic transition (dashed lines) in the upper mantle. Some earlier faults, although depicted here as soling out in ductile lower crust, may have reached similar depths. (b) Persisting slip on the normal fault. Unlike conditions associated with earlier faulting, the rift is relatively amagmatic, so that thermal weakening does not engender a new fault elsewhere in the rift valley. Fault slip probably is facilitated by reduction in friction coefficient due to serpentinization and other effects (see text). (c) Continued fault slip leading to mantle exposure. The footwall rolls over and is deformed by subvertical simple shear and/or flexural failure (Figure 13). Melt generated from renewed magmatism in the rift valley or by decompression melting deep in the footwall intrudes the footwall and forms volcanic cones or flows on its surface. (d) End of megamullion formation. A southward propagating rift terminates slip on the detachment fault; the rift propagation may be facilitated by thermal weakening associated with magmatism noted in Figure 12c.

mullion structures are congruent from near the breakaway to the termination; it is unlikely that these same structures would have persisted if other detachments had incised the footwall or been excised into the hanging wall. We found no offsets in the megamullion surface that might indicate the mullions are created by normal faulting orthogonal to isochrons, as suggested by *Karson* [1999]. The continuity of the mullions suggests that they were formed by persistent irregularities in the fault trace [*Tucholke et al.*, 1998], possibly by "continuous casting" of deformable rock [*Spencer*, 1999].

The domed shape of the megamullion shows that the footwall must have deformed significantly as it was exhumed. The active detachment fault probably was at the edge of the rift valley (Figure 12), but the fault dip is poorly known. Our observations noted above, together with Andersonian faulting theory and observed earthquake focal mechanisms for teleseismic events in ocean crust [*Thatcher and Hill*, 1995], suggest that the fault probably dipped at ~45°–60°. The fault surface on the

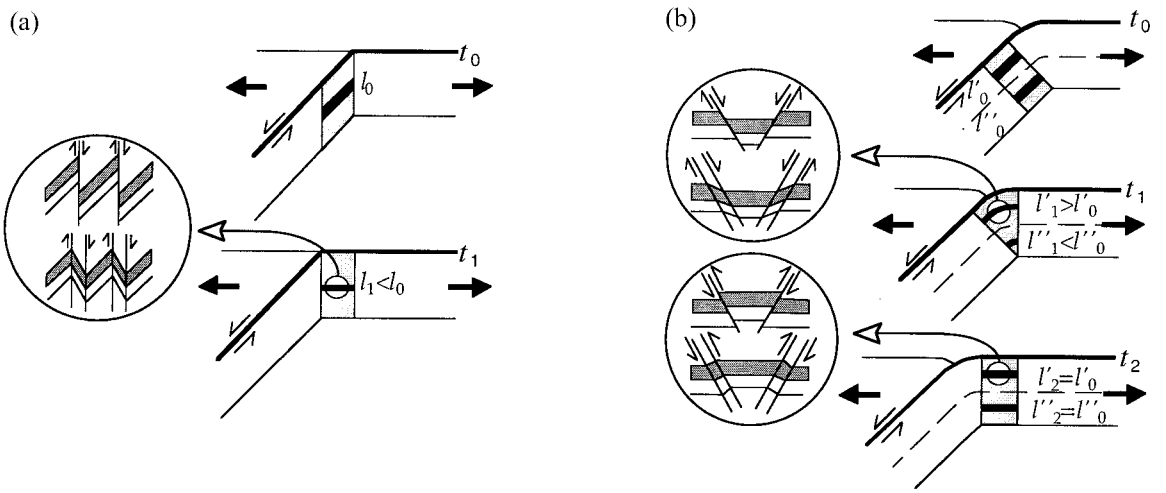

Figure 13. Schematic cross sections showing possible modes of deformation of a detachment footwall in a "rolling hinge," adapted from *Manning and Bartley* [1994]. (a) Subvertical simple shear. (b) Flexural failure. Line elements l (bold lines) parallel the foliation at times t_0 to t_2 in the deformed volume indicated by shading. The neutral surface in the beam is indicated by a dashed line. Insets show associated patterns of brittle strain.

eastern side of the domes dips ~10° away from the ridge axis (Figure 11), so its total rotation could be of the order of 55° or more. Brittle deformation of the footwall could be expected to occur either as subvertical simple shear in dominantly outward facing (away from the spreading axis) high-angle normal faults or by flexural failure on conjugate inward and outward facing faults (Figure 13) [*Manning and Bartley*, 1994; *Axen and Bartley*, 1997]. Within 6–8 km west of the breakaway, seafloor morphology shows a number of east facing scarps ~50–100 m high (Figures 2 and 3). We infer that these scarps represent subvertical simple shear in brittle crust.

Over the main domes, there is no evidence for large-scale, isochron-parallel offsets greater than a few tens of meters (Figure 2). If subvertical simple shear was important here, it most likely occurs as pervasive, small-scale deformation. The same is true if flexural failure occurred, except that reverse faulting on the outboard side of the hinge could have reduced the throw of originally larger-offset normal faults (Figure 13b, bottom). The vertical fluid flow suggested by heat flow measurements over the megamullion dome (Figure 10) provides indirect evidence that the footwall may be pervasively fractured and permeable. The difference in seafloor morphology between the domes and the lithosphere closer to the breakaway, both in terms of mullion development and occurrence of isochron-parallel scarps (Figures 2 and 3), suggests that rheology of the footwall rocks is very different between the two areas. One possible explanation is that the domes contain substantial amounts of readily deformed serpentinite. Brittle fracture of mantle ultramafics as they were exhumed through temperatures <500°C in the bending footwall could have created numerous pathways for fluid flow and caused substantial serpentinization [e.g., *Macdonald and Fyfe*, 1985]. Subsequent deformation of these weak rocks in the shallower part of the hinge might be distributed rather than focused in large normal faults like those that intersect the detachment surface closer to the breakaway.

The cause of long-lived slip on the detachment fault is uncertain. For the fault to persist, the sum of the frictional and plate flexure stresses must be less than the total cohesional and frictional stresses that would be required to break a new fault [*Forsyth*, 1992; *Buck*, 1993]. There are a number of possible effects that might significantly reduce friction coefficient on the fault; these include serpentinization [*Reinen et al*., 1994; *Moore et al*., 1997; *Escartín et al*., 1997], changes in deformation mechanism associated with grain-size reduction [*Jaroslow et al*., 1996], elevated pore fluid pressure [e.g., *Byerlee*, 1990; *Axen*, 1992; *Rice*, 1992; *Karson*, 1999], or melt interaction in the shear zone below the brittle-plastic transition [*Dick et al*., 1991; *Hopkinson and Roberts*, 1995; *Kelemen and Dick*, 1995]. For these effects to be important in long-lived detachment faults, they would have to persist for periods of ~1.0–2.6 m.y. (the observed durations of megamullion detachments [*Tucholke et al*., 1998]) before changes in conditions beneath the rift axis permitted breaking a new fault. The effects of serpentinization and changes in deformation mechanism could well persist for such long periods, and they may be pivotal to reducing friction coefficient and promoting continued fault slip. The effects of pore fluid pressure and melt interaction, however, may not be consistent enough over these timescales to assure that strain remains localized on one fault.

By itself, reduced friction coefficient on the fault does not explain other aspects of megamullions, such as their limited frequency of occurrence or the termination of their development. Long-lived detachment faults that form megamullions are not common, and these features form only a small fraction of all IC highs. In contrast, conditions thought to be necessary for serpentinization and grain-size reduction on faults in slow spreading crust are widespread. Observed deep seismicity at the ridge axis [*Toomey et al*., 1988; *Bergman and Solomon*, 1990; *Kong et al*., 1992; *Wolfe et al*., 1995], for example, suggests a high incidence of fault pathways where water may reach and serpentinize the mantle. This appears to be confirmed by the frequent recovery of serpentinites by dredge and submersible, particularly in IC tectonic settings [e.g., *Cannat et al*., 1992, 1995; *Tucholke and Lin*, 1994]. From these observations we expect that megamullions should be much more common if serpentinization along faults was the sole control on their development. In addition, while the friction-reducing effects of serpentinites may help to explain why detachment faults slip

for long periods, they do not explain why the faults cease to slip after periods of 1.0–2.6 m.y.

One possible way to resolve these discrepancies is to consider that the occurrence and longevity of major detachment faults may be limited by the distribution and cyclicity of magmatism at the ridge axis. Ridge flank studies of gravity and relative crustal thickness have shown that magmatism appears to wax and wane with a period of ~2–3 m.y. [*Tucholke and Lin*, 1994; *Pariso et al*., 1995; *Tucholke et al*., 1997]. Megamullion formation usually correlates with the less magmatic parts of these cycles [*Tucholke et al*., 1998], that is, at times when fault penetration to the mantle is most likely to occur and fault weakening by serpentinization may be enhanced. This is the situation at Dante's Domes. RMBA gravity is elevated along isochrons within the spreading segment at the location where the main megamullion domes developed (Figure 4), and serpentinites recovered from the RMBA high during dive 440 show that mantle was exhumed at least locally. Both features indicate that melt input during megamullion formation was limited compared with crustal formation at earlier and later times.

The megamullion may have ceased to develop as a result of increased magmatism following the less magmatic phase during which the bulk of the feature formed. The residual gravity anomaly decreases and relative crustal thickness increases throughout the spreading segment in younger crust. The only in-place volcanics found over the surface of Dante's Domes were observed on the west flank during dive 438, suggesting an increase in magmatism within ~0.3 m.y. of the termination (Figure 12). Associated thermal weakening of rift valley lithosphere could have promoted propagation of the rift that arrested megamullion formation between ~1.3 and 0.7 Ma. We consider it unlikely that the volcanics were emplaced as a result of the rift propagation itself because they occur at large distances (up to at least 5 km) from the trace of the propagator.

Although termination of the megamullion appears to correlate with a segment-wide increase in magmatism, there may be an additional effect related to the thermal structure of the megamullion itself. If more heat is advected upward in the exhumed footwall than is lost by conduction, isotherms will be elevated, and decompression melting may be stimulated beneath the rift axis (Figures 12c and 12d). Melt migration into the upper part of the footwall could be enhanced by compression in the lower part of the footwall below the neutral plane of the bending plate and by extension in the upper part (Figure 13b, middle). Ultimately, thermal weakening of the rift valley lithosphere caused by the migrating melt could stimulate formation of a new primary fault or facilitate rift propagation. In this way the cycle of megamullion development might be self-limiting. It is presently unclear whether this phenomenon, if it occurs, is of primary importance to megamullion termination or is secondary to the effects of broader magmatic cycles noted above.

The actual level of magmatism during megamullion formation is difficult to quantify, although it is reduced compared with younger and older crust and clearly is not robust, as suggested by *Karson* [1999]. Because an identifiable magnetic anomaly sequence appears over the megamullion (Figures 1 and 11), there must be some magmatic component in the footwall. It is not necessary that the magnetization contrasts responsible for these anomalies be within extrusive crust. In a detailed study of magnetization on the flank of the Mid-Atlantic Ridge, *Tivey and Tucholke* [1998] found that magnetization in the extrusives is attenuated rapidly off axis, and they suggested that most of the remaining ridge flank magnetization is within the lower crust. Thus, in the case of Dante's Domes, magnetization recording the polarity reversal history may reside within intrusive crust or within intrusives in peridotite/serpentinite screens as envisioned by *Cannat* [1993]. Either interpretation is permissible within the constraints of the gravity modeling (Figure 9), which suggests that intermediate densities predominate throughout most of the megamullion dome.

6. Conclusions

Five submersible dives, combined with surface ship geophysical data, constrain the structure and origin of Dante's Domes megamullion in the rift mountains on the east flank of the Mid-Atlantic Ridge near 26°35′N. The megamullion appears to be the footwall of a long-lived, normal detachment fault that initiated ~2.0–2.2 Ma at the edge of the rift valley and was terminated between 1.3 and 0.7 Ma by southward transit of a propagating rift. The breakaway where the fault originated is marked by prominent ridges 400–600 m high. The east face of the main ridge (ridge B in Figures 3 and 11) is a volcanic depositional slope that has been rotated eastward by up to 50°–60°; the west face of the ridge is interpreted to contain the detachment fault responsible for exhumation of Dante's Domes megamullion. Along the *Shinkai* dive transect a slightly younger breakaway probably occurs along the west face of ridge A (Figures 3 and 11). However, this fault merges to the north and south with the older fault, and ridge A appears to be a rider block above the primary detachment. Although some eastward rotation of the blocks constituting ridges A and B can be explained by isostatic rebound, most of the rotation probably occurred as the blocks slipped above an underlying, older shear zone.

West of the breakaway, the detachment fault surface rises to form a pair of broad, gently sloping domes aligned along isochrons. Elevated residual mantle Bouguer gravity centered on the megamullion and along strike within the enclosing spreading segment indicates that the megamullion formed during a period of reduced magmatic activity, compared with preceding and subsequent crustal accretion. Serpentinites were sampled from the RMBA high, and modeling of sea surface and seafloor gravity measurements also shows that higher-than-normal densities occur in this location, confirming that the oceanic crust is thin or missing along the central part of the megamullion.

Dive observations show that the detachment surface is extremely smooth and is thinly covered by sediment and scattered allochthonous basalts that are interpreted to have been clipped from the hanging wall. We observed no faults or other high-angle perturbations that correlate with low-amplitude (tens of meters) mullion structures and isochron-parallel scarps defined by sea surface multibeam bathymetry. The footwall must have deformed as it was exhumed and bowed to form the domes, but this appears to have been accommodated by pervasive small-scale deformation rather than by large-scale faulting. If serpentinized peridotite is widely distributed within the domes, this weak material may help to explain the lack of megascopic deformation. Large east facing scarps up to ~100 m high appear east of the domes and within 6–8 km of the breakaway; they may be created by subvertical simple shear in more brittle, igneous crust.

Our observations of gravity, structure, and lithology suggest

that the Dante's Domes detachment fault was active during a period of reduced magmatism and that it was abandoned when magmatic activity increased. Increased magmatism toward the termination of the megamullion is indicated by the appearance of small pillow basalt cones and other minor in-place flows on the detachment surface. The increased magmatism may have been part of a natural magmatic cycle, or it may have been stimulated by decompression melting in the rising footwall, or both. Accompanying thermal weakening of the rift valley lithosphere could have facilitated propagation of the rift that terminated slip on the detachment fault.

Modeling of sea surface and seafloor gravity measurements indicates that mantle densities occur within ~1.5 km of the seafloor ~3–6 km west of the breakaway. That observation and the recovery of serpentinites a short distance to the west suggest that the detachment fault originally dipped ≥45° in the rift valley, assuming that it cut through normal thickness ocean crust. The dip may have been lower if it cut through thinner crust. Other than the shallow mantle wedge that seems to be required on the east side of the dome, the exact nature and distribution of lithologies in the megamullion is uncertain. Serpentinized peridotite, gabbroic plutons, and/or intrusives within serpentinite/peridotite screens would match the intermediate densities suggested by gravity modeling. The presence of low-amplitude but identifiable magnetic anomalies over the megamullion indicates that there is at least some intrusive component in the footwall. Detailed near-bottom surveys and drilling will be needed to resolve the complex characteristics of footwall lithology.

Acknowledgments. B. Tucholke's research was supported by NSF grant OCE-9503561 and by an award from the Andrew W. Mellon Foundation Endowed Fund for Innovative Research and the Henry Bryant Bigelow Chair in Oceanography at Woods Hole Oceanographic Institution. G. Hirth acknowledges support by NSF grant OCE-9907244. We thank the officers and crew of R/V *Yokosuka* for outstanding support during the MODE-98 dive program on Dante's Domes. We also thank our MODE-98 scientific colleagues and R. P. Von Herzen, J. Lin, and H. J. B. Dick for helpful discussions and L. Dolby for technical assistance. Contribution 10440 of Woods Hole Oceanographic Institution.

References

Auzende, J.-M., M. Cannat, P. Gente, J.-P. Henriet, T. Juteau, J. Karson, Y. Lagabrielle, C. Mével, and M. Tivey, Observation of sections of oceanic crust and mantle cropping out on the southern wall of Kane FZ (N. Atlantic), *Terra Nova*, *6*, 143–148, 1994.

Axen, G. J., Pore pressure, stress increase, and fault weakening in low-angle normal faulting, *J. Geophys. Res*., *97*, 8979–8991, 1992.

Axen, G. J., and J. M. Bartley, Field tests of rolling hinges: Existence, mechanical types, and implications for extensional tectonics, *J. Geophys. Res*., *102*, 20,515–20,537, 1997.

Becker, K., and R. P. Von Herzen, Pre-drilling observations of conductive heat flow at the TAG active mound using ALVIN, *Proc. Ocean Drill. Program Initial Rep*., *158*, 23–29, 1996.

Bergman, E. A., and S. C. Solomon, Earthquake swarms on the Mid-Atlantic Ridge: Products of magmatism or extensional tectonics?, *J. Geophys. Res*., *95*, 4943–4965, 1990.

Blackman, D. K., J. R. Cann, B. Janssen, and D. K. Smith, Origin of extensional core complexes: Evidence from the Mid-Atlantic Ridge at Atlantis Fracture Zone, *J. Geophys. Res*., *103*, 21,315–21,333, 1998.

Bredehoeft, J. D., and I. S. Papadopulos, Rates of vertical groundwater movement estimated from the Earth's thermal profile, *Water Resour. Res*., *1*, 325–328, 1965.

Buck, W. R., Effect of lithospheric thickness on the formation of high- and low-angle normal faults, *Geology*, *21*, 933–936, 1993.

Bullard, E. C., Heat flow in South Africa, *Proc. R. Soc. London*, *Ser. A*, *173*, 474–502, 1939.

Byerlee, J. D., Friction, overpressure and fault normal compression, *Geophys. Res. Lett*., *17*, 2109–2112, 1990.

Cann, J. R., D. K. Blackman, D. K. Smith, E. McAllister, B. Janssen, S. Mello, E. Avgerinos, A. R. Pascoe, and J. Escartín, Corrugated slip surfaces formed at ridge-transform intersections on the Mid-Atlantic Ridge, *Nature*, *385*, 329–332, 1997.

Cannat, M., Emplacement of mantle rocks in the seafloor at mid-ocean ridges, *J. Geophys. Res*., *98*, 4163–4172, 1993.

Cannat, M., D. Bideau, and H. Bougault, Serpentinized peridotites and gabbros in the Mid-Atlantic Ridge axial valley at 15°37′N and 16°52′N, *Earth Planet. Sci. Lett*., *109*, 87–106, 1992.

Cannat, M., et al., Thin crust, ultramafic exposures, and rugged faulting patterns at the Mid-Atlantic Ridge (22°–24°N), *Geology*, *23*, 49–52, 1995.

Collins, J. A., and R. S. Detrick, Seismic structure of the Atlantis Fracture Zone megamullion, a serpentinized ultramafic massif, *Eos Trans. AGU*, *79*(45), Fall Meet. Suppl., F800, 1998.

Davis, E. E., Oceanic heat-flow density, in *Handbook of Terrestrial Heat-Flow Density Determination*, edited by R. Haenel, L. Rybach, and L. Stegena, pp. 223–260, Kluwer Acad., Norwell, Mass., 1988.

Davis, G. A., and G. S. Lister, Detachment faulting in continental extension: Perspectives from the southwestern U.S. Cordillera, in *Processes in Continental Lithosphere Deformation*, *Spec. Pap. Geol. Soc. Am*., *218*, 133–159, 1988.

Dick, H. J. B., P. S. Meyer, S. Bloomer, S. Kirby, D. Stakes, and C. Mawer, Lithostratigraphic evolution of an in-situ section of oceanic layer 3, *Proc. Ocean Drill. Program Sci. Results*, *118*, 439–538, 1991.

Escartín, J., G. Hirth, and B. Evans, Effects of serpentinization on the lithospheric strength and the style of normal faulting at slow-spreading ridges, *Earth Planet. Sci. Lett*., *151*, 181–189, 1997.

Forsyth, D. W., Finite extension and low-angle normal faulting, *Geology*, *20*, 27–30, 1992.

Hammer, S., Terrain corrections for gravity stations, *Geophysics*, *4*, 184–194, 1939.

Harrison, C. G. A., Marine magnetic anomalies—The origin of the stripes, *Annu. Rev. Earth Planet. Sci*., *15*, 505–543, 1987.

Hopkinson, L., and S. Roberts, Ridge axis deformation and coeval melt migration within layer 3 gabbros: Evidence from the Lizard Complex, U. K., *Contrib. Mineral. Petrol*., *121*, 126–138, 1995.

Howard, K. A., and B. E. John, Crustal extension along a rooted system of imbricate low-angle faults: Colorado River extensional corridor, California and Arizona, in *Continental Extensional Tectonics*, edited by M. P. Coward, J. F. Dewey and P. L. Hancock, *Geol. Soc. Spec. Publ. 28*, 299–311, 1987.

Jaroslow, G. E., The geological record of oceanic crustal accretion and tectonism at slow-spreading ridges, Ph.D. thesis, 210 pp., Mass. Inst. of Technol.—Woods Hole Oceanogr. Inst. Joint Program in Oceanogr., Woods Hole, Mass., 1997.

Jaroslow, G. E., G. Hirth, and H. J. B. Dick, Abyssal peridotite mylonites: Implications for grain-size sensitive flow and strain localization in the oceanic lithosphere, *Tectonophysics*, *256*, 17–37, 1996.

Karson, J. A., Geological investigation of a lineated massif at the Kane Transform Fault: Implications for oceanic core complexes, *Philos. Trans. R. Soc. London*, *357*, 713–740, 1999.

Kelemen, P. B., and H. J. B. Dick, Focused melt flow and localized deformation in the upper mantle: Juxtaposition of replacive dunite and ductile shear zones in the Josephine peridotite, SW Oregon, *J. Geophys. Res*., *100*, 423–438, 1995.

Kong, L. S., S. C. Solomon, and G. M. Purdy, Microearthquake characteristics of a mid-ocean ridge along-axis high, *J. Geophys. Res*., *97*, 1659–1685, 1992.

Kuo, B. Y., and D. W. Forsyth, Gravity anomalies of the ridge-transform system in the South Atlantic between 31° and 34.5°S: Upwelling centers and variations in crustal thickness, *Mar. Geophys. Res*., *10*, 205–232, 1988.

Macdonald, A. H., and W. S. Fyfe, Rate of serpentinization in seafloor environments, *Tectonophysics*, *116*, 123–135, 1985.

Manning, A. H., and J. M. Bartley, Postmylonitic deformation in the Raft River metamorphic core complex, northwestern Utah: Evidence of a rolling hinge, *Tectonics*, *13*, 596–612, 1994.

Minshull, T. A., Along-axis variations in oceanic crustal density and their contribution to gravity anomalies at slow-spreading ridges, *Geophys. Res. Lett*., *23*, 849–852, 1996.

Mitchell, N. C., J. Escartín, and S. Allerton, Detachment faults at mid-ocean ridges garner interest, *Eos Trans. AGU*, *79*, 127, 1998.

Moore, D. E., D. A. Lockner, M. Shengli, R. Summers, and J. D. Byerlee, Strengths of serpentinite gouges at elevated temperatures, *J. Geophys. Res*., *102*, 14,787–14,801, 1997.

Pariso, J. E., J.-C. Sempéré, and C. Rommevaux, Temporal and spatial variations in crustal accretion along the Mid-Atlantic Ridge (29°–31°30′N) over the last 10 m.y.: Implications from a three-dimensional gravity study, *J. Geophys. Res*., *100*, 17,781–17,794, 1995.

Parker, R. L., The rapid calculation of potential anomalies, *Geophys. J. R. Astron. Soc*., *31*, 447–455, 1972.

Parsons, B., and J. G. Sclater, An analysis of the variation of ocean floor bathymetry and heat flow with age, *J. Geophys. Res*., *82*, 803–827, 1977.

Reinen, L. A., J. D. Weeks, and T. E. Tullis, The frictional behavior of lizardite and antigorite serpentinites: Experiments, constitutive models, and implications for natural faults, *Pure Appl. Geophys*., *143*, 318–358, 1994.

Rice, J. R., Fault stress states, pore pressure distributions, and the weakness of the San Andreas Fault, in *Fault Mechanics and Transport Properties of Rocks*: *A Festschrift in Honor of W. F. Brace*, edited by B. Evans and T. Wong, pp. 475–503, Academic, San Diego, Calif., 1992.

Shaw, P. R., Ridge segmentation, faulting and crustal thickness in the Atlantic Ocean, *Nature*, *358*, 490–493, 1992.

Spencer, J. E., Geologic continuous casting below continental and deep-sea detachment faults and at the striated extrusion of Sacsayhuamán, Peru, *Geology*, *27*, 327–330, 1999.

Talwani, M., C. C. Windisch, and M. G. Langseth, Reykjanes Ridge crest: A detailed geophysical study, *J. Geophys. Res*., *76*, 473–517, 1971.

Thatcher, W., and D. P. Hill, A simple model for the fault-generated morphology of slow spreading mid-ocean ridges, *J. Geophys. Res*., *100*, 561–570, 1995.

Tivey, M. A., Vertical magnetic structure of ocean crust determined from near-bottom magnetic field measurements, *J. Geophys. Res*., *101*, 20,275–20,296, 1996.

Tivey, M. A., and B. E. Tucholke, Magnetization of 0 to 29 Ma ocean crust on the Mid-Atlantic Ridge at 25°30′ to 27°10′N, *J. Geophys. Res*., *103*, 17,807–17,826, 1998.

Toomey, D. R., S. C. Solomon, and G. M. Purdy, Microearthquakes beneath the median valley of the Mid-Atlantic Ridge near 23°N: Tomography and tectonics, *J. Geophys. Res*., *93*, 9093–9112, 1988.

Tucholke, B. E., and J. Lin, A geological model for the structure of ridge segments in slow spreading ocean crust, *J. Geophys. Res*., *99*, 11,937–11,958, 1994.

Tucholke, B. E., J. Lin, and M. C. Kleinrock, Mullions, megamullions, and metamorphic core complexes on the Mid-Atlantic Ridge (abstract), *Eos Trans. AGU*, *77*(46), Fall Meet. Suppl., F724, 1996.

Tucholke, B. E., J. Lin, M. A. Tivey, M. C. Kleinrock, T. B. Reed, J. A. Goff, and G. E. Jaroslow, Segmentation and crustal structure of the western Mid-Atlantic Ridge flank, 25°25′–27°10′N and 0–29 m.y., *J. Geophys. Res*., *102*, 10,203–10,223, 1997.

Tucholke, B. E., J. Lin, and M. C. Kleinrock, Megamullions and mullion structure defining oceanic metamorphic complexes on the Mid-Atlantic Ridge, *J. Geophys. Res*., *103*, 9857–9866, 1998.

Wolfe, C. J., G. M. Purdy, D. R. Toomey, and S. C. Solomon, Microearthquake characteristics and crustal velocity structure at 29°N on the Mid-Atlantic Ridge: The architecture of a slow spreading segment, *J. Geophys. Res*., *100*, 24,449–24,472, 1995.

K. Fujioka and M. Kinoshita, Japan Marine Science and Technology Center, 2–15, Natsushima-cho, Yokusuka, Kanagawa Prefecture 237, Japan. (fujiokak@jamstec.go.jp; masa@jamstec.go.jp)

G. Hirth and B. E. Tucholke, Department of Geology and Geophysics, Woods Hole Oceanographic Institution, Woods Hole, MA 02543-1541. (ghirth@whoi.edu; btucholke@whoi.edu)

T. Ishihara, Institute for Marine Resources and Environment, National Institute for Advanced Industrial Science and Technology, AIST Tsukuba Central 7, Tsukuba, 305-8567 Japan. (t-ishihara@aist.go.jp)

(Received March 10, 2000; revised December 15, 2000;
accepted March 14, 2001.)